

Article

Physical Simulation on Weakly Cemented Aquiclude Stability due to Underground Coal Mining

Shizhong Zhang ^{1,2}, Gangwei Fan ^{1,*}, Dongsheng Zhang ¹, Tao Luo ¹, Xue Guo ¹, Siqin Dun ¹ and Hua Chen ¹¹ School of Mines, China University of Mining and Technology, Xuzhou 221116, China² School of Resources and Earth Science, China University of Mining and Technology, Xuzhou 221116, China

* Correspondence: fangw@cumt.edu.cn; Tel.: +86-13655203693

Abstract: In northwest China, underground mining is frequently conducted in weakly cemented rock environments, including the aquiclude that protects the aquifer from dewatering. In this context, understanding the aquiclude responses to longwall mining is significant for assessing the reliability of water-conserved mining in the weakly cemented rock environment. Taking the Jurassic and Paleogene coal measure geology in Yili Mine in Xinjiang Province, China, as a case study, the paper conducted a laboratorial three-dimensional simulation by configuring a longwall operation and induced groundwater migration. The study analysed the aquiclude depressurisation and revealed the aquiclude stability in response to longwall mining. The results indicated that the aquiclude had a significant plastic strain and self-healing ability in the ground depressurisation condition. The aquiclude experienced tension and then compression, and, accordingly, fracture initiation, propagation, and convergence, during which the aquiclude had significant bending deformation. On the aquiclude horizon, tensile fracturing dominated above the set-up and longwall stop positions. The self-healing behaviour was correlated to the high content of clay minerals and disintegration proneness. The simulation results had a good agreement with field measurements, suggesting that the aquiclude had a satisfactory water-resisting ability and that the simulation results were practically reliable.

Keywords: water-conserved mining; weakly cemented rocks; aquiclude stability; self-healing behaviour; physical simulation



Citation: Zhang, S.; Fan, G.; Zhang, D.; Luo, T.; Guo, X.; Dun, S.; Chen, H. Physical Simulation on Weakly Cemented Aquiclude Stability due to Underground Coal Mining. *Minerals* **2022**, *12*, 1494. <https://doi.org/10.3390/min12121494>

Academic Editor: Robert Šajn

Received: 11 October 2022

Accepted: 22 November 2022

Published: 23 November 2022

Publisher's Note: MDPI stays neutral with regard to jurisdictional claims in published maps and institutional affiliations.



Copyright: © 2022 by the authors. Licensee MDPI, Basel, Switzerland. This article is an open access article distributed under the terms and conditions of the Creative Commons Attribution (CC BY) license (<https://creativecommons.org/licenses/by/4.0/>).

1. Introduction

The aquiclude above the longwall panels blocks the overlying aquifer water from flowing downward into goaf voids [1–3]. In coal measure geology, the aquiclude is deformed, fractured and likely to be destabilised by longwall mining, hence becoming less capable of preventing aquifer dewatering [4–6]. In northwest China, underground coal mining mainly occurs in Jurassic and Paleogene formations, where the rocks are generally characterised by young sedimentation, low strength, weak cementation, and high proneness of disintegration in hydrous conditions [7]. The arid and semi-arid climate results in a fragile environment in which the mine ecology highly depends on the shallow aquifer. Reportedly, in local areas, the mining activities have caused extensive fracturing and aquiclude destabilisation, followed by surface water leakage, desertification, and vegetation degradation [8–11]. In this condition, exploiting coal resources with minor impact on the regional water system has become a challenge for the mining industry [12]. The first knowledge to be consolidated is a thorough understanding of the aquiclude stability mechanism in such weakly cemented rock environment. Addressing this problem can form a basis for evaluating the impact of future longwall projects and longwall system design.

Studies have been conducted on the weakly cemented rock physics and mechanics [13–15]. Yu et al. analysed the impact of water content and confining pressure on the failure pattern and stress-strain trajectory of weakly cemented mudstones

(WCM), indicating that the WCM mechanical responses were correlated to the physical and structural properties; in this study, the impact of rock porosity, mineral composition, and matrix-pore continuity on WCM strength was analysed. Wang and Zhao et al. proposed that the water-rock interaction, clay mineral disintegration, and particle expansion had a major contribution to the WCM failure and strength reduction [16,17]. Wang et al. quantified the correlation of the WCM bulk density and P-wave velocity versus uniaxial compressive strength and elastic modulus through laboratorial tests and theoretical analysis [18]. Li and Zhao et al. studied the WCM stress-strain, acoustic emission, and energy variations in a Brazilian test and discussed their relationship [19,20]. Some scholars also studied the joint strength and the coupled seepage-damage effect of natural fractured rock masses [21,22]. A previous study by the authors investigated the WCM permeability variation in complete stress-strain and post-peak loading and unloading conditions, revealing a WCM permeability property, regarding the high initial permeability, and minor differences between the peak and initial permeabilities [23,24]. Existing studies have obtained the physical and mechanical properties of the WCM aquiclude, but have not focused on the mechanisms of aquiclude deformation, fracturing, and destabilisation caused by longwall mining.

Some studies on the aquiclude stability have focused primarily on the roof claystone aquiclude and floor competent aquiclude [25–27]. Huang and Fan et al. identified the good water-resisting ability of red soils and claystones and that the fracture convergence was mainly because of rock matrix bulking in the fluid flow environment [28,29]. Yu and Ma proposed that adopting a roadway backfilling method can help control the deformation and settlement of the red soil aquiclude, through which the natural water-resisting ability can be well maintained [30]. Zhang and Sun et al. analysed the mechanism of claystone aquiclude destabilisation and aquifer dewatering in the backfill mining condition, proposing that the regional water resource can be protected by reconstructing the key aquiclude [31,32]. Feng, Fu, and Wang et al. proposed that the water-resisting property of the floor aquiclude mainly depends on both the structural and permeability stability, based on which the impact of lithology, aquiclude thickness, and water pressure on the floor aquiclude stability was analysed [33–35]. Liu et al. identified that the existence of water-conducting collapse pillars can directly decrease the effective water-resisting thickness of the floor aquiclude and thus increase the floor water inrush potentials [36]. These studies identified an ordinary mechanism of the roof claystone aquiclude and floor aquiclude destabilisation due to longwall mining, but have not considered the impact of the aquiclude lithology, such as weakly cemented rocks, on the stability. In order to understand this problem, a physical scaled model was constructed in this paper considering its advantages in explicitly reflecting the overlying strata deformation and fracturing due to panel extraction [37–40].

This paper took the Jurassic and Paleogene coal measure geology in the Yili No. 4 Coal Mine, Xinjiang Province, China, as a case study, of which the lithology is mainly characterised by weakly cemented rocks. A self-developed three-dimensional simulation system was employed to model the coal measure geology and analyse the WCR aquiclude fracturing and aquifer dewatering during panel extraction. Further, the aquiclude destabilisation mechanism was analysed from the mineral composition and water-rock interaction perspectives. The research results can provide a reference for water-conserved mining practices in the weakly cemented rock environment.

2. Study Site

The Yili No. 4 Coal Mine is located in Yining, Xinjiang Province, northwest China. The region has an arid to semi-arid climate, with annual precipitation ranging between 186.3 and 387.7 mm, resulting in a fragile ecology. The shallow gravel aquifer belongs to Quaternary formations, mainly recharged by precipitation and snowmelt. Under the aquifer is a Paleogene mudstone aquiclude and deeper Jurassic coal measure strata. The study area was the first longwall panel (LW21103) of this mine. LW21103 has a mining height of 3.5 m, a panel width of 115 m, and a depth of cover 115 m, on average, and the

coal seam is near horizontal. The shallow aquifer is 10 m thick and 20 m in depth, providing water for the mine ecology. The aquiclude is 5 m thick, on average, with an 85 m distance to the panel roof. Figure 1 exhibits the coal measure lithology and thickness.

STRATUM	COLUMN	LITHOLOGY	THICKNESS	REMARK
Quaternary (Q)		Silt layer	20 m	
		Gravel layer	10 m	Aquifer
Paleogene (E)		Mudstone	5 m	Aquiclude
		Sandstone	50 m	
		Mudstone	10 m	
Jurassic (J)		Sandstone	10 m	
		Mudstone	10 m	
		21-1 Coal seam	3.5 m	Mining thickness
		Mudstone	25 m	

Figure 1. Coal measure lithology of LW21103.

3. Physical Simulation

A physical simulation was conducted to capture the WCM aquiclude responses to longwall panel extraction. The physical simulation was configured for LW21103 coal measure lithology using a self-developed device. Longwall retreat mining was simulated, during which the aquiclude displacement and groundwater drawdown were monitored.

3.1. Method

The physical simulation adopted a 3D non-destructive fluid-solid coupling test system, developed by the authors [41], as shown in Figure 2. The non-destructive fluid-solid coupling test system abandoned the traditional data monitoring method by buried depth sensors in physical models, which solved the problems of original rock stress state and surrounding rock integrity damage caused by the buried depth sensors. The system used a parallel electrical system to trace groundwater migration by monitoring anomalies of apparent resistivity. The model of the parallel electrical system was YBD11 with six base stations and 96 excitation channels. The measuring current accuracy was 0.5%, and the minimum sampling interval was 1 ms. The panel extraction was configured by varying the height of hydraulic jacks; through the servo-control system, the mining height can be precisely adjusted with a 0.1 cm gradient. The model was 290 cm in length, 150 cm in width, and 115 cm in height, it was geometrically 1:100, with respect to the in-situ geometry. In addition, the time similarity ratio was 1:10. Table 1 lists the type and quality of various materials applied to the physical simulation.

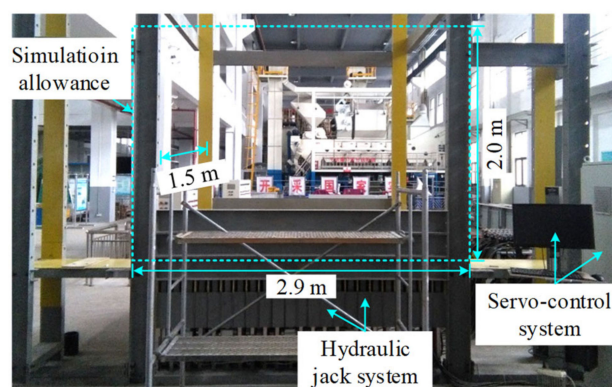


Figure 2. 3D non-destructive fluid-solid coupling test system.

Table 1. Type and quality of materials used in physical simulation.

Lithology	UCS /MPa	Sand /kg	CaCO ₃ (Bentonite) /kg	Gypsum /kg	Paraffin /kg	Water /kg	Notes
Silts	3.0	-	-	-	-	-	Replaced by soil
Gravels	3.0	658.13	51.19	21.94	-	8.00	Shallow aquifer
Mudstone	10.0	325.00	36.56 (bentonite)	4.06	12.19	4.00	Aquiclude
Sandstone	15.2	3290.63	255.94	109.69	73.13	40.00	
Mudstone	10.0	639.84	63.98 (bentonite)	27.42	18.28	8.00	
Sandstone	12.4	658.13	51.19	21.94	14.63	8.00	
Mudstone	10.0	639.84	63.98 (bentonite)	27.42	18.28	800	
21-1 coal	3.0	-	-	-	-	-	Dropping the jacks

Note: bentonite (containing clay minerals) was used for mudstones.

3.2. Process

Before the panel extraction was performed, the monitoring points and devices for the aquiclude displacement and groundwater migration were installed, coupled with parallel electrical surveying points, as shown in Figure 3.

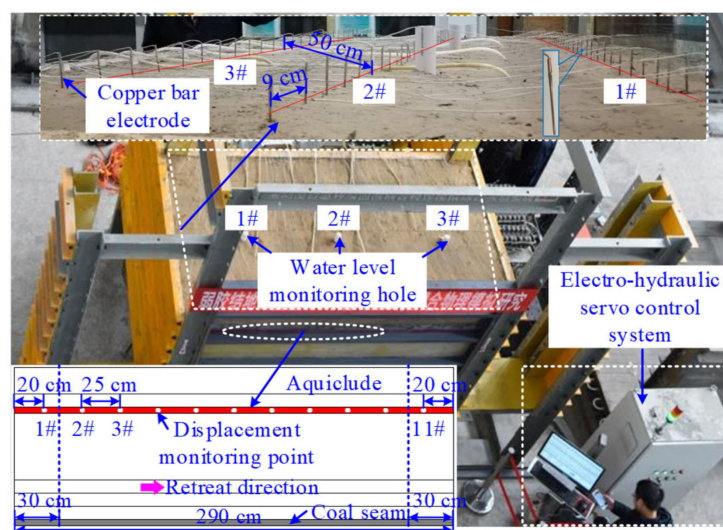


Figure 3. Measurement configuration.

(1) Aquiclude displacement monitoring

The monitoring points were placed in the middle of the aquiclude, starting from 20 cm to the left edge, with a 25 cm spacing. There were 11 monitoring points in total.

(2) Groundwater flow monitoring

Three piezometers were vertically placed on the upper surface of the model, extending to the aquifer bottom. Piezometer 1# and 3# were 45 cm to the lateral edges, and piezometer 2# was in the middle and 100 cm to piezometers 1# and 3#, respectively, and 50 cm to the frontal surface. The three piezometers were used to inject water into the shallow aquifer before mining and to monitor the water level during mining.

(3) Parallel electrical surveying

Parallel electrical surveying points were placed on the top surface of the model, incorporating three surveying lines with 50 cm distance. Line 2# was the model centreline along the width direction, and line 1# and 3# were, respectively, 25 cm to the frontal and back surface. Each surveying line included 32 points with a 9 cm spacing. The copper electrodes were embedded 1 cm below the top surface.

Before the longwall mining, a transparent plexiglass plate was installed along the frontal surface, replacing the previous metal plate, to assist in capturing the strata deformation and fracturing. In addition, transparent silicone grease and butter materials were applied to each surface around the model to make it well sealed. The simulated longwall

distance was 230 cm, leaving a 30 cm wide section unmined on each lateral to eliminate potential impacts of boundaries. This design corresponded to the in-situ 230 m longwall progress. The actual retreat speed of the coalface was 10 m/d. In order to restore the actual mining process of the coalface to the greatest extent in the excavation of the physical model, each mining step of the physical model extracted a 10 cm length with a time interval of 144 min, according to geometric similarity and temporal similarity. The longwall mining process of the physical model begins at the left side, as shown in Figure 3. In addition, the extraction of the coal seam was configured by varying the height of the hydraulic jacks by the servo-control system.

3.3. Results

3.3.1. Aquiclude Fracturing

Figure 4 shows the aquiclude fracturing during longwall mining progress.

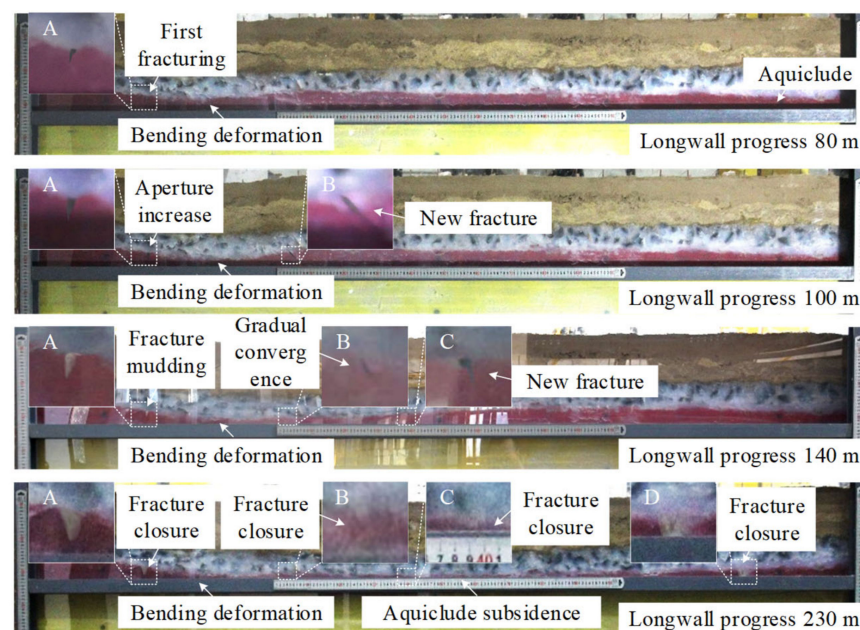


Figure 4. Variation of aquiclude fracture initiation, propagation, and convergence.

Figure 4 shows that the aquiclude had a significant bending deformation as the longwall mining progressed 80 m, accompanied by a small-scale subsidence trough formed above. In this stage, a minor fracture (A) was captured above the set-up position due to the horizontal tension impact on the aquiclude.

When the longwall progressed 100 m, the aquiclude continuously subsided, accompanied by an increase in the fracture (A) aperture. In this condition, the fracture had not extended to the aquiclude bottom. Another tensile fracturing occurred above the current longwall workface position, labelled B in Figure 4.

After a further 40 m longwall progress, the previous tensile fracture (A) started to converge as it gradually filled with disintegrated clay minerals. Another fracture (B) had a similar phenomenon, represented by a pronounced aperture decrease. A new aquiclude fracture (C) was initiated above the current workface position.

After finalising the panel extraction, the aquiclude showed significant deflection above both the set-up and longwall stop positions. In contrast, the middle part mainly characterised a coordinated settlement. In this case, the tensile fractures A and D were closed due to the clay mineral fillings, while fractures B and C also converged due to the full settlement. Figure 5 exhibits the post-mining scenario.

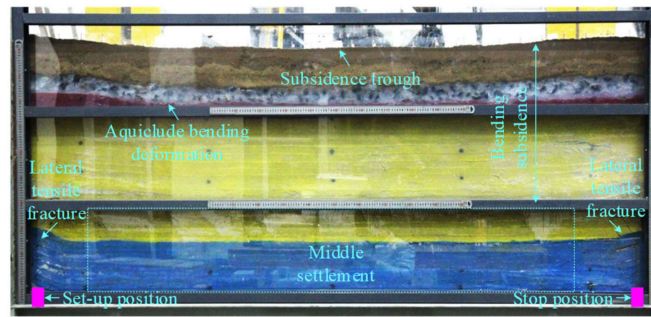


Figure 5. Post-mining overburden movement profile in the weakly cemented rock environment.

The above analysis indicated that the WCM aquiclude behaved as a good resistance to the plastic deformation, of which the bending deformation dominated. Above the goaf voids, the aquiclude was tensioned and then compressed, thus representing a variation regarding fracture initiation, propagation, and closure. Above the set-up and longwall stop positions, the aquiclude mainly characterised tensile fracturing, also exhibiting the progress of fracture initiation, propagation, and convergence.

3.3.2. Aquiclude Displacement

Figure 6 shows the aquiclude displacement during panel extraction.

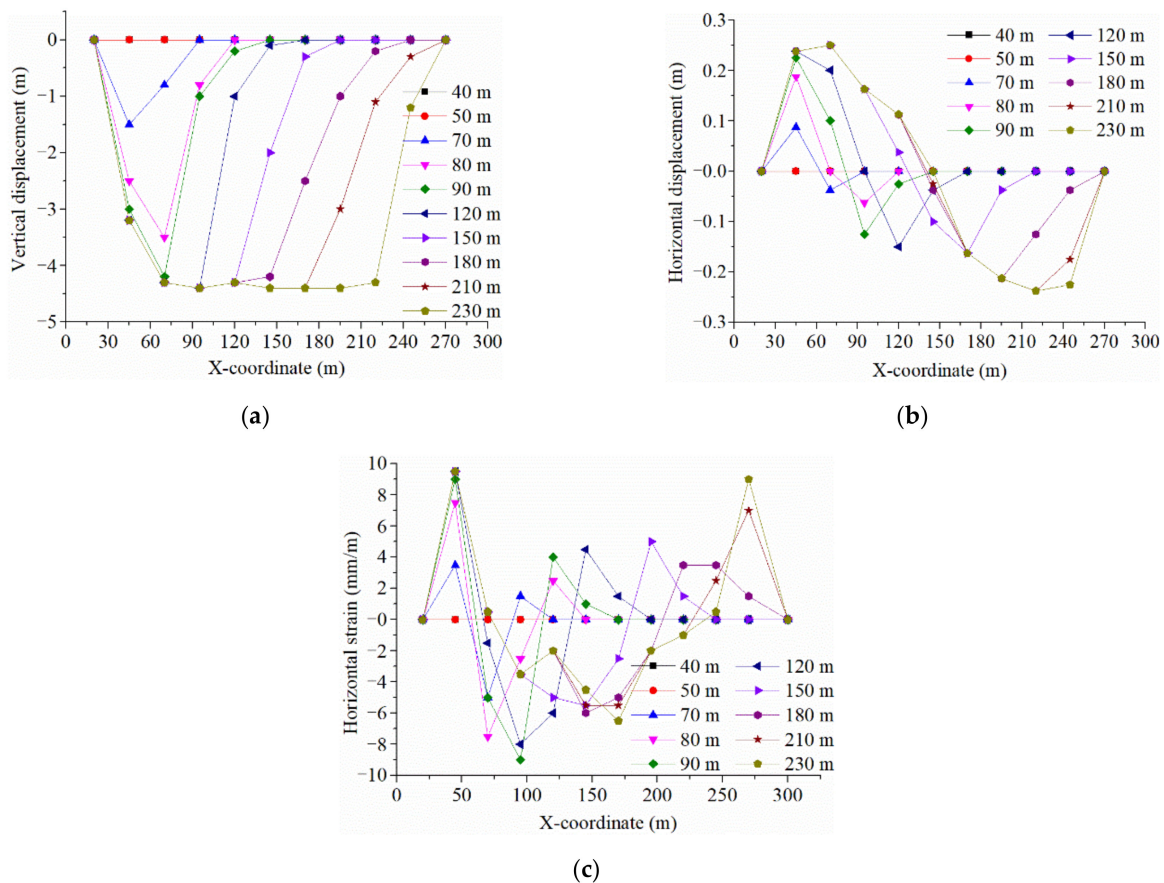


Figure 6. Aquiclude displacement during panel extraction: (a) vertical displacement; (b) horizontal displacement; (c) horizontal strain.

As can be seen from Figure 6, the longwall impact on the aquiclude displacement was explicitly observed when the workface marched 70 m. In this condition, the vertical displacement at measuring point 2# was -1.5 m, horizontal displacement 0.088 m, and

horizontal strain 3.5 mm/m. With further longwall progress, the displacement variation rate (at measuring point 2#) first increased, and then gradually levelled off to 0. The displacement at measuring point 2# reached the maximum, -3.2 m for vertical displacement and 0.238 m for horizontal displacement, when the longwall progressed 120 m.

Measuring points 3# and 9# had a similar displacement variation as point 2#, as the panel was further extracted. A difference among the various measurements was the displacement direction; the aquiclude displaced towards right at left side, as recorded by measuring point 2#, and displaced towards the left on the right side, by measuring point 10#. By contrast, at the middle measuring points (3# to 9#) the aquiclude moved left at first and then right.

After the panel extraction was finalised, the maximum vertical displacement of the aquiclude was -4.4 m, with a subsidence coefficient of 0.88. The maximum horizontal displacement and strain of the aquiclude were around the set-up and longwall stop positions, respectively, 0.238 m and 9.5 mm/m. The maximum horizontal displacement occurred at the edge of the subsidence trough, where the aquiclude was horizontally stretched and thus had a greater displacement. Compared to this position, the trough centre had a minor horizontal displacement, at almost 0.

3.3.3. Groundwater Flow

(1) Water level variation

Figure 7 shows the water level responses to the continuous panel extraction.

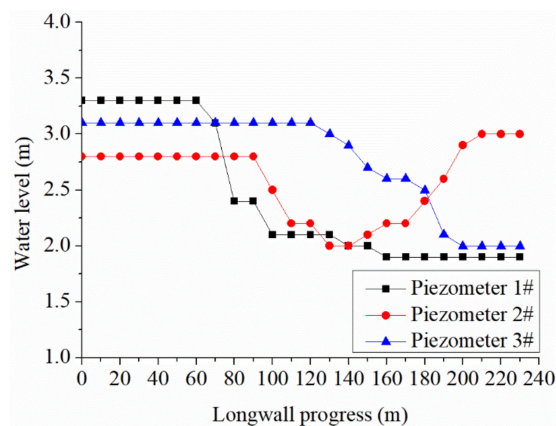


Figure 7. Water level responses to the continuous longwall progress.

Before the longwall mining, the three piezometers observed that the depth of water level was 3.3, 2.8, and 3.1 m, respectively. After the longwall progressed 70 m, piezometer 1# recorded a water level drawdown of 0.2 m. After a further 10 m longwall progress, the water level declined to 2.4 m, and, correspondingly, an accelerated drawdown of 22.6%. Then, the drawdown became much more gradual and ultimately levelled off, causing the original water level to be declined, overall, by 1.4 m, approximately 42.4% of the original level.

Piezometer 2# recorded a water level drawdown of 0.3 m when the longwall progressed 100 m, which is later than for piezometer 1#. The water level at piezometer 2# reached the minimum value 2.0 m after the longwall progressed 130 m, favouring a maximum drawdown of 0.8 m, 28.6% of the original water level. However, in the case of the 150 m longwall progress, the water level of piezometer 2# increased by 0.1 m, then rose further to 3.0 m, with the longwall progressing 210 m and ultimately maintained. The recovered water level was higher than the original value, by 0.2 m. According to the model, the reason why the water level of piezometer 2# rose was that it was located in the middle of the subsidence basin. In the later stage of the experiment, the groundwater on both sides of the subsidence basin converged to the middle, causing the water level of piezometer 2# to be higher than its initial value.

Piezometer 3# had a similar water level variation to piezometer 1#, recording a maximum drawdown of 1.1 m when the longwall progressed 200 m; 1.1 m smaller than the maximum drawdown recorded by piezometer 1#. The maximum drawdown at piezometer 3# was 35.5% of the original level.

(2) Apparent resistivity

Apparent resistivity can help reflect groundwater storage in localised areas. Considering the electrical conductivity of water, the area where water accumulates should have a low electrical resistivity. A ratio of the post-mining resistivity to pre-mining resistivity was defined to explicitly capture any minor variation, namely apparent resistivity anomaly index (ARAI). Figure 8 shows the ARAI profile after the panel extraction was finalised.

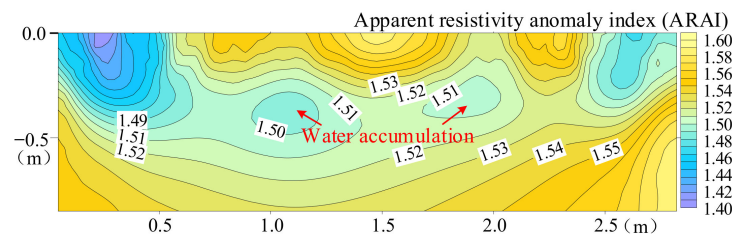


Figure 8. ARAI profile of the overlying strata.

As can be seen in Figure 8, there were two low ARAI areas above the goaf void, indicating a localised groundwater accumulation in both areas. Combining the aquiclude displacement profile indicated that both low ARAI areas were in the middle of the subsidence trough. Simultaneously, the aquiclude and strata below had high ARAIs, implying that the aquiclude still had a satisfactory water-resisting competence and that the overlying groundwater was partially maintained above the aquiclude. The results implied that the aquifer was well protected from extensive dewatering.

4. Discussion

The physical simulation indicated that the WCM aquiclude fractured due to longwall mining, whereas the fracture partially converged in the water seepage environment. This can be considered a self-healing ability of the WCM lithology. To understand the mechanism of WCM aquiclude responses to longwall mining, the paper further analysed the contribution of mineral composition and water-rock interaction to the WCM aquiclude stability from chemical and mechanical perspectives. The test samples were taken from the Paleogene mudstone aquiclude of Yili No. 4 Coal Mine.

4.1. Mineral Composition

The WCM mineral composition was observed using X-ray diffractometer (Type D8 ADVANCE); the results are shown in Figure 9.

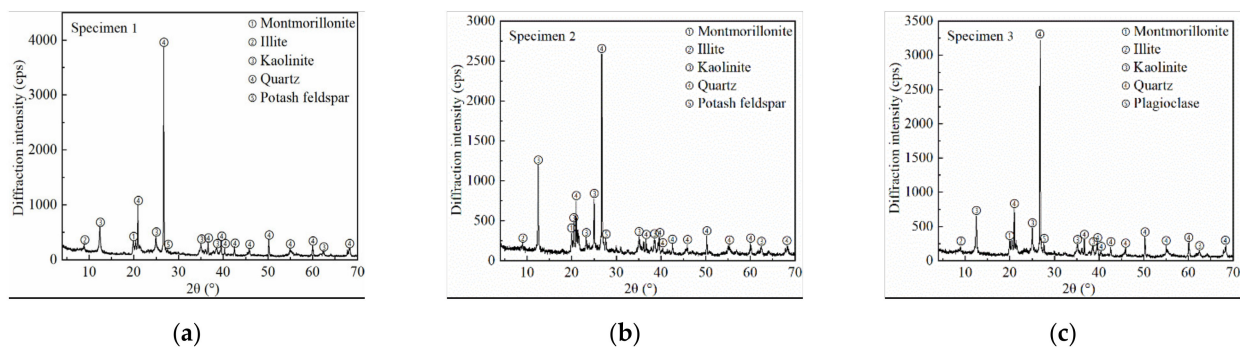


Figure 9. X-ray diffraction patterns of weakly cemented mudstone: (a) Specimen 1; (b) Specimen 2; (c) Specimen 3.

Table 2 Summaries the WCM mineral composition obtained from Figure 9.

Table 2. Mineral composition of weakly cemented mudstone.

Specimen	Mineral Composition and Proportion (%)						Clay Minerals (%)
	Quartz	Kaolinite	Montmorillonite	Illite	Plagioclase	Potash Feldspar	
1#	31.0	48.2	13.8	4.8	0.0	2.2	66.8
2#	20.6	55.8	14.6	3.5	0.0	5.5	73.9
3#	30.1	49.3	13.2	3.7	3.7	0.0	66.2
Average	27.2	51.1	13.9	4.0	1.2	2.6	69.0

Table 2 shows that the weakly cemented mudstones were mainly dominated by Quartz, Kaolinite, and Montmorillonite, making up 92.2% of the total content. In addition, there was a small quantity of Illite, Plagioclase, and Potash feldspar, forming 7.8% of the total content, on average. Among these minerals, Kaolinite possessed the highest content, 51.5%; followed by Quartz (27.2%) and Montmorillonite (13.9%). The three clay minerals, Kaolinite, Montmorillonite, and Illite, possessed 69%, two times of other minerals. Considering that clay minerals behave significant volumetric expansion after encountering water, a knowledge widely accepted by academics [42–44], the aquiclude fractures thus exhibited a gradual convergence in the water seepage environment, demonstrating a self-healing ability.

4.2. Water-Rock Interaction

The paper further studied the water-rock interaction of weakly cemented mudstone in hydrous conditions. A WCM specimen was submerged into distilled water in a beaker, before which a 7 mm wide fracture was fabricated on the specimen surface to test the fracture convergence in response to clay mineral argillisation and expansion. The use of distilled water could truly reflect the water-rock interaction of weakly cemented aquiclude after encountering water and excluded the influence of chemical ions. Figure 10 exhibits the water-rock interaction effect and fracture aperture variation with time.

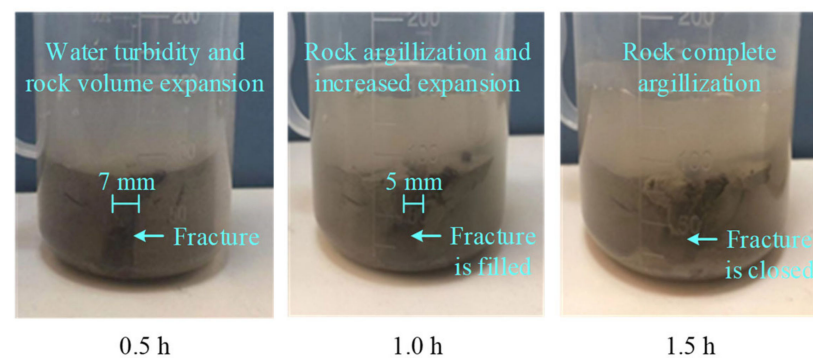


Figure 10. Water-rock interaction effect on the WCM specimen and fracture variation with time.

Figure 10 shows that the water started to be turbid after 0.5 h, accompanied by evident rock expansion and almost no change in the fracture aperture. The rock expansion and argillisation became significant after 1.0 h, and the prefabricated fracture converged to 5 mm, with the bottom part filled with rock fragments. After 1.5 h, the argillisation was complete, causing the rock to become severely deformed and the water to become further turbid. In this stage, the fracture was entirely closed. The results indicate that the weakly cemented mudstone had pronounced volumetric expansion and argillisation after being submerged in water for 1.5 h, during which the fracture can be filled with rock fragments. In contrast, ordinary rocks such as sandstone, limestone, and granite can remain intact in hydrous conditions for tens or even hundreds of days [45,46]. As analysed, the weakly cemented mudstones had a unique property regarding the volumetric expansion and

argillisation when encountering water, thus giving this lithology an ability to heal mining-induced fractures. This property made a positive contribution to the aquiclude stabilisation in longwall mining practice.

5. Field Test

In the case mine, a piezometer was installed on the ground, 1265 m away from the LW21103 set-up position, to record the groundwater level. The piezometer was above the LW21103 belt roadway and drilled to the bottom of the gravel aquifer, as shown in Figure 11. Figure 12 shows the groundwater depressurisation and recovery as the workface passed the monitoring position (labelled 0 x-coordinate). The original water level was marked 0.

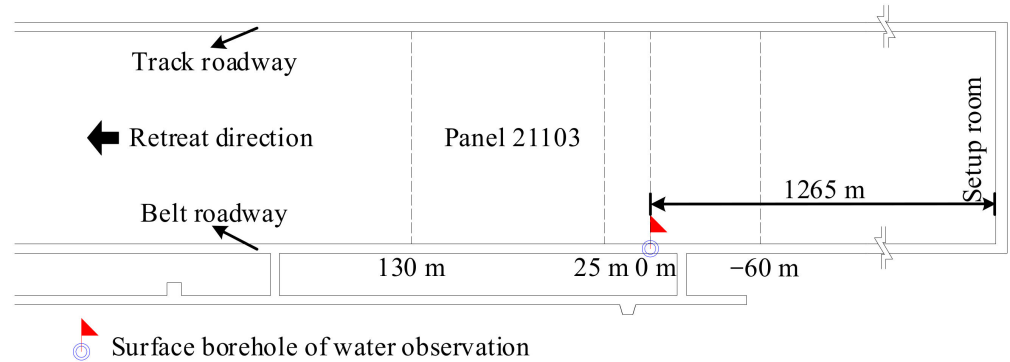


Figure 11. Piezometer position with respect to LW21103 workings.

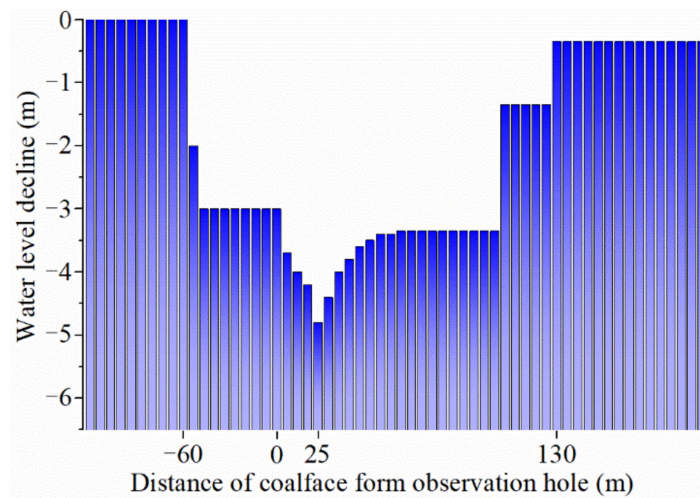


Figure 12. Groundwater level variation with longwall progress.

Figure 12 shows that the piezometer captured the first groundwater depressurisation, as the workface was 60 m ahead of the monitoring position. This can be attributed to the longwall’s impact on the frontal areas; the water flowed to the subsidence trough above the mined-out area; accordingly, the recorded water level declined. The water level continued to drop with the longwall progress, reaching -3.0 m as the workface was just below the piezometer, and reaching the lowest, at -4.8 m, when the workface was 25 m beyond the piezometer. After 130 m of longwall progress, the water level gradually recovered to the maximum due to water recharges from the river and snowmelt. This variation indicated that the WCM aquiclude remained stable and possessed a good water-resisting functionality during the longwall mining process. It can be considered that LW21103 operated a water-conserved mining, which agreed with the physical simulation results.

6. Conclusions

A solid-fluid coupling simulation was conducted using a self-developed non-destructive testing platform, demonstrating that the WCM aquiclude was dominated by a bending deformation in response to the longwall mining. The aquiclude above the mined-out areas was tensioned and then compressed, accompanied by evident fracture initiation, propagation, and convergence. Above the set-up and longwall stop positions, the main characteristic of the aquiclude was tensile fracturing, experiencing a process of fracture initiation, propagation, and closure. This variation implied that the WCM aquiclude had a significant ability for plastic deformation and self-healing.

The self-healing ability of weakly cemented mudstones was correlated to the rich clay minerals, as well as to the argillisation and disintegration behaviour in the water environment. The volumetric expansion and argillisation proneness of the clay minerals in the hydrous environment allowed the mining-induced fractures to be narrowed. The water-rock interaction caused weakly cemented mudstones to be completely decomposed in 1.5 h, further facilitating the closure of the aquiclude fractures.

In-situ piezometric monitoring showed that the shallow aquifer water experienced a temporary drawdown, due to longwall mining, and then a recovery, due to water recharges from the river and snowmelt. The water level variation indicated that the WCM aquiclude maintained its water-resisting functionality, and that the monitored panel achieved water-conserved mining. This measurement had a good agreement with the physical simulation, implying a satisfactory reliability of the research results.

Author Contributions: Conceptualization, S.Z. and G.F.; methodology, D.Z.; validation, T.L. and X.G.; data curation, S.D. and H.C.; writing—original draft preparation, S.Z.; writing—review and editing, G.F. and D.Z. All authors have read and agreed to the published version of the manuscript.

Funding: This research was funded by the National Natural Science Foundation of China (Grant No. 52204161; 51974291), the Fundamental Research Funds for the Central Universities (Grant No. 2022QN1008; 2021ZDPY0226), the Jiangsu Funding Program for Excellent Postdoctoral Talent (Grant No. 2022ZB511), the Shanxi Province Unveils Bidding Project (Grant No. 20201101009).

Data Availability Statement: Not applicable.

Acknowledgments: The authors are grateful to the anonymous reviewers for their helpful comments.

Conflicts of Interest: The authors declare no conflict of interest.

References

1. Booth, C.J.; Curtiss, A.M.; Demaris, P.J.; Bauer, R.A. Site-specific variation in the potentiometric response to subsidence above active longwall mining. *Environ. Eng. Geosci.* **2000**, *6*, 383–394. [[CrossRef](#)]
2. Sun, Y.-J.; Xu, Z.-M.; Dong, Q.-H.; Liu, S.-D.; Gao, R.-B.; Jiang, Y.-H. Forecasting water disaster for a coal mine under the Xiaolangdi reservoir. *J. China Univ. Min. Technol.* **2008**, *18*, 516–520. [[CrossRef](#)]
3. Liu, J.; Zhao, Y.; Tan, T.; Zhang, L.; Zhu, S.; Xu, F. Evolution and modeling of mine water inflow and hazard characteristics in southern coalfields of China: A case of Meitanba mine. *Int. J. Min. Sci. Technol.* **2022**, *32*, 513–524. [[CrossRef](#)]
4. Zhou, Q.; Herrera-Herbert, J.; Hidalgo, A. Predicting the risk of fault-induced water inrush using the adaptive neuro-fuzzy inference system. *Minerals* **2017**, *7*, 55. [[CrossRef](#)]
5. Zhang, S.; Fan, G.; Zhang, D.; Li, Q. Physical simulation research on evolution laws of clay aquifuge stability during slice mining. *Environ. Earth Sci.* **2018**, *77*, 278. [[CrossRef](#)]
6. Imaykin, A.; Imaykin, K. The hydrodynamic regime of underground and mine waters in the process and after the cessation of underground mining of the reserves of the shumikhinskoye coal deposit. In Proceedings of the 18 International Multidisciplinary Scientific GeoConference SGEM 2018, Sofia, Bulgaria, 2–8 July 2018; Volume 18, pp. 683–690. [[CrossRef](#)]
7. Zhang, S.; Fan, G.; Zhang, D.; Chen, M.; Zhang, C. Study on material properties and similar material proportion of weakly cemented water-resisting strata. *Arab. J. Geosci.* **2019**, *12*, 340. [[CrossRef](#)]
8. Zhang, D.; Fan, G.; Ma, L.; Wang, X. Aquifer protection during longwall mining of shallow coal seams: A case study in the Shandong Coalfield of China. *Int. J. Coal Geol.* **2011**, *86*, 190–196. [[CrossRef](#)]
9. Shepley, M.G.; Pearson, A.D.; Smith, G.D.; Banton, C.J. The impacts of coal mining subsidence on groundwater resources management of the East Midlands Permo-Triassic Sandstone aquifer, England. *Q. J. Eng. Geol. Hydrogeol.* **2008**, *41*, 425–438. [[CrossRef](#)]
10. Santana, C.S.; Montalván Olivares, D.M.; Silva, V.H.C.; Luzardo, F.H.M.; Velasco, F.G.; de Jesus, R.M. Assessment of water resources pollution associated with mining activity in a semi-arid region. *J. Environ. Manag.* **2020**, *273*, 111148. [[CrossRef](#)]

11. Obiadi, I.I.; Obiadi, C.M.; Akudinobi, B.E.B.; Maduewesi, U.V.; Ezim, E.O. Effects of coal mining on the water resources in the communities hosting the Iva Valley and Okpara Coal Mines in Enugu State, Southeast Nigeria. *Sustain. Water Resour. Manag.* **2016**, *2*, 207–216. [[CrossRef](#)]
12. Zhang, S.; Fan, G.; Zhang, D.; Li, S.; Chen, M.; Fan, Y.; Luo, T. Impacts of longwall mining speeds on permeability of weakly cemented strata and subsurface watertable: A case study. *Geomat. Nat. Hazards Risk* **2021**, *12*, 3063–3088. [[CrossRef](#)]
13. Dong, J.; Tu, C.; Lee, W.; Jheng, Y. Effects of hydraulic conductivity/strength anisotropy on the stability of stratified, poorly cemented rock slopes. *Comput. Geotech.* **2012**, *40*, 147–159. [[CrossRef](#)]
14. Erguler, Z.A.; Karakuş, H.; Ediz, I.G.; Şensöğüt, C. Assessment of design parameters and the slope stability analysis of weak clay-bearing rock masses and associated spoil piles at Tunçbilek basin. *Arab. J. Geosci.* **2020**, *13*, 41. [[CrossRef](#)]
15. Kadir, S.; Akbulut, A. Occurrence of sepiolite in the hirsizdere sedimentary magnesite deposit, Bozkurt-Denizili, SW Turkey. *Carbonates Evaporites* **2001**, *16*, 17–25. [[CrossRef](#)]
16. Zhao, Z.; Liu, H.; Lyu, X.; Wang, L.; Tian, Z.; Sun, J. Experimental study on the damage and deterioration behaviour of deep soft rock under Water-Rock Interaction. *Geofluids* **2021**, *2021*, 8811110. [[CrossRef](#)]
17. Wang, S.; Han, L.; Meng, Q.; Jin, Y.; Zhao, W. Investigation of pore structure and water imbibition behavior of weakly cemented silty mudstone. *Adv. Civ. Eng.* **2019**, *2019*, 8360924. [[CrossRef](#)]
18. Wang, Z.; Li, W.; Wang, Q.; Liu, S.; Hu, Y.; Fan, K. Relationships between the petrographic, physical and mechanical characteristics of sedimentary rocks in Jurassic weakly cemented strata. *Environ. Earth Sci.* **2019**, *78*, 131. [[CrossRef](#)]
19. Zhao, Y.; Liu, B. Deformation field and acoustic emission characteristics of weakly cemented rock under brazilian splitting test. *Nat. Resour. Res.* **2021**, *30*, 1925–1939. [[CrossRef](#)]
20. Li, P.; Li, Z.-H.; Liu, B.; Teng, T.; Guo, J.-T. Experimental investigation on the tensile properties of weakly cemented sandstone in China Shendong mining area. *Therm. Sci.* **2020**, *24*, 3987–3994. [[CrossRef](#)]
21. Zhao, Y.; Zhang, C.; Wang, Y.; Lin, H. Shear-related roughness classification and strength model of natural rock joint based on fuzzy comprehensive evaluation. *Int. J. Rock Mech. Min. Sci.* **2021**, *137*, 104550. [[CrossRef](#)]
22. Zhao, Y.; Liu, Q.; Zhang, C.; Liao, J.; Lin, H.; Wang, Y. Coupled seepage-damage effect in fractured rock masses: Model development and a case study. *Int. J. Rock Mech. Min. Sci.* **2021**, *144*, 104822. [[CrossRef](#)]
23. Fan, G.; Chen, M.; Zhang, D.; Wang, Z.; Zhang, S.; Zhang, C.; Li, Q.; Cao, B. Experimental study on the permeability of weakly cemented rock under different stress states in triaxial compression tests. *Geofluids* **2018**, *2018*, 9035654. [[CrossRef](#)]
24. Liang, S.; Zhang, D.; Fan, G.; Guo, W.; Gao, S.; Zhang, S.; Fan, Z.; Yu, W. Aquiclude stability evaluation and significance analysis of influencing factors of close-distance coal seams: A case study of the Yili No. 4 coal mine in Xinjiang, China. *Geofluids* **2021**, *2021*, 3518271. [[CrossRef](#)]
25. Wang, X.; Zhu, W.; Xu, J.; Han, H.; Fu, X. Mechanism of overlying strata structure instability during mining below unconsolidated confined aquifer and disaster prevention. *Appl. Sci.* **2021**, *11*, 1778. [[CrossRef](#)]
26. Liu, S.; Li, W.; Qiao, W.; Li, X.; Wang, Q.; He, J. Zoning method for mining-induced environmental engineering geological patterns considering the degree of influence of mining activities on phreatic aquifer. *J. Hydrol.* **2019**, *578*, 124020. [[CrossRef](#)]
27. Islam, M.R.; Shinjo, R. Mining-induced fault reactivation associated with the main conveyor belt roadway and safety of the Barapukuria Coal Mine in Bangladesh: Constraints from BEM simulations. *Int. J. Coal Geol.* **2009**, *79*, 115–130. [[CrossRef](#)]
28. Huang, Q.X. Research on Cracks Zone of Clay Aquiclude in Overburden. In *Applied Mechanics and Materials*; Trans Tech Publications Ltd.: Zurich, Switzerland, 2014; Volume 548–594, pp. 1744–1747. [[CrossRef](#)]
29. Fan, Z.; Fan, K.; Liu, Z.; Feng, Y.; Wei, H.; Zhou, Y. Experimental study on the mining-induced water-resistance properties of clay aquicludes and water conservation mining practices. *Adv. Civ. Eng.* **2021**, *2021*, 4868998. [[CrossRef](#)]
30. Yu, Y.; Ma, L. Application of roadway backfill mining in water-conservation coal mining: A case study in Northern Shaanxi, China. *Sustainability* **2019**, *11*, 3719. [[CrossRef](#)]
31. Sun, Q.; Zhang, J.; Li, M.; Zhou, N. Experimental evaluation of physical, mechanical, and permeability parameters of key aquiclude strata in a typical mining area of China. *J. Clean. Prod.* **2020**, *267*, 122109. [[CrossRef](#)]
32. Zhang, J.; Sun, Q.; Li, M.; Zhao, X. The mining-induced seepage effect and reconstruction of key aquiclude strata during backfill mining. *Mine Water Environ.* **2019**, *38*, 590–601. [[CrossRef](#)]
33. Fu, B.; Zhang, H.; Tu, M.; Zhang, X. Deformation and stress distribution of the effective water-resisting rock beam under water-rock coupling action inside the panel floor. *Adv. Civ. Eng.* **2018**, *2018*, 2157097. [[CrossRef](#)]
34. Feng, M.; Mao, X.; Bai, H. Influence of Confined Water on Water Insulating Effect of Water-Resisting Strata in Seam Flood. In *Progress In Safety Science and Technology, Proceedings of the 2010 International Symposium on Safety Science and Technology, Hangzhou, China, 26–29 October 2010*; Beijing Institute of Technology: Beijing, China, 2010; pp. 2558–2565.
35. Wang, J.A.; Park, H.D. Coal mining above a confined aquifer. *Int. J. Rock Mech. Min. Sci.* **2003**, *40*, 537–551. [[CrossRef](#)]
36. Liu, H.; Li, L.; Li, Z.; Yu, G. Numerical modelling of mining-induced inrushes from subjacent water conducting karst collapse columns in northern China. *Mine Water Environ.* **2018**, *37*, 652–662. [[CrossRef](#)]
37. Xu, S.; Zhang, Y.; Shi, H.; Zhang, Z.; Chen, J. Impacts of aquitard properties on an overlying unconsolidated aquifer in a mining area of the loess plateau: Case study of the Changcun Colliery, Shanxi. *Mine Water Environ.* **2020**, *39*, 121–134. [[CrossRef](#)]
38. Wang, P.; Jiang, L.; Li, X.; Qin, G.; Wang, E. Physical simulation of mining effect caused by a fault tectonic. *Arab. J. Geosci.* **2018**, *11*, 741. [[CrossRef](#)]

39. Sun, Q.; Meng, G.; Sun, K.; Zhang, J. Physical simulation experiment on prevention and control of water inrush disaster by backfilling mining under aquifer. *Environ. Earth Sci.* **2020**, *79*, 429. [[CrossRef](#)]
40. Li, A.; Ji, B.; Ma, Q.; Ji, Y.; Mu, Q.; Zhang, W.; Mu, P.; Li, L.; Zhao, C. Physical simulation study on grouting water plugging of flexible isolation layer in coal seam mining. *Sci. Rep.* **2022**, *12*, 875. [[CrossRef](#)]
41. Zhang, D.; Fan, G.; Liang, S.; Ma, L.; Wang, X.; Zhang, W.; Zhang, S. 3D non-destructive monitoring system for solid-liquid coupling of mining-induced overburden and its application. *J. Min. Saf. Eng.* **2019**, *36*, 1071–1078. [[CrossRef](#)]
42. Al-Rawas, A.A.; Guba, I.; McGown, A. Geological and engineering characteristics of expansive soils and rocks in northern Oman. *Eng. Geol.* **1998**, *50*, 267–281. [[CrossRef](#)]
43. Doostmohammadi, R.; Moosavi, M.; Araabi, B.N. A model for determining the cyclic swell—Shrink behavior of argillaceous rock. *Appl. Clay Sci.* **2008**, *42*, 81–89. [[CrossRef](#)]
44. Kohno, M. Effects of hydraulic gradient and clay type on permeability of clay mineral materials. *Minerals* **2020**, *10*, 1064. [[CrossRef](#)]
45. Luo, T.; Fan, G.; Guo, B.; Zhang, S. Experimental study on the influence of hydro-chemical erosion on morphology parameters and shear properties of limestone fractures. *Acta Geotech.* **2021**, *16*, 3867–3880. [[CrossRef](#)]
46. Liu, Y.; Li, J.; Wu, Y.; Lv, S. Study on the effect of acidic environment on mechanical properties of rock. *Sci. Technol. Eng.* **2017**, *17*, 196–201.